Valence band density of states of zinc-blende and wurtzite InN from x-ray photoemission spectroscopy and first-principles calculations

P. D. C. King, T. D. Veal, and C. F. McConville*
Department of Physics, University of Warwick, Coventry CV4 7AL, United Kingdom

F. Fuchs, J. Furthmüller, and F. Bechstedt
Institut für Festkörpertheorie und -Optik, Friedrich-Schiller-Universität, Max-Wien-Platz 1, D-07743 Jena, Germany

J. Schörmann, D. J. As, and K. Lischka
Department Physik, Universität Paderborn, Warburger Strasse 100, 33098 Paderborn, Germany

Hai Lu† and W. J. Schaff
Department of Electrical and Computer Engineering, Cornell University, Ithaca, New York 14853, USA
(Received 17 January 2008; published 26 March 2008)

The valence band density of states (VB-DOS) of zinc-blende InN(001) is investigated using a combination of high-resolution x-ray photoemission spectroscopy and quasiparticle corrected density functional theory. The zinc-blende VB-DOS can be characterized by three main regions: a plateau region after the initial rise in the DOS, followed by a shoulder on this region and a second narrow but intense peak, similar to other III-V and II-VI semiconductor compounds. Good general agreement was observed between the experimental and theoretical results. Tentative evidence for an *s-d* coupling due to the interaction between valence-like N 2*s* states and semicore-like In 4*d* states is also identified. Measurements and calculations for wurtzite InN($11\bar{2}0$) are shown to yield a VB-DOS similar to that of zinc-blende InN, although the nonzero crystal field and different Brillouin zone shape in this case lead to a more complicated band structure which modifies the DOS. In adlayers terminating the InN($11\bar{2}0$) surface are also evident in the experimental VB-DOS, and these are discussed.

DOI: 10.1103/PhysRevB.77.115213 PACS number(s): 71.20.Nr, 79.60.−i, 71.15.Mb

I. INTRODUCTION

Indium nitride (InN) remains the least understood semiconductor of the group-III nitride material system, although it has been intensely investigated in recent years, largely due to its narrow band gap[1,2] and excellent predicted transport characteristics.[3] While the thermodynamically stable phase is the wurtzite 2*H* polymorph[4] (wz-InN), judicious choice of substrate material and orientation allows growth of the zinc-blende 3*C* polymorph (zb-InN).[5–8] It is thought that zb-InN may be preferable for potential device applications due to the smaller predicted band gap[4] and higher degree of symmetry, removing the anisotropy present in wurtzite structures and hence reducing phonon scattering, although structural quality is unlikely to be as high as for wz-InN.

The electronic structure of zb-InN has previously been the subject of a number of theoretical investigations,[4,9–12] but limitations in growth quality of single-crystal zb-InN samples have largely prevented detailed experimental electronic studies. Recently, however, growth of zb-InN on 3*C*-SiC(001) substrates incorporating a zb-GaN buffer layer was reported with only 5% wurtzite inclusions and zb-InN(002) x-ray rocking curve widths of less than 50 arc min.[7] From photoluminescence spectra, a low temperature band gap of 0.61 eV (Ref. 7) was estimated for zb-InN, somewhat lower than for wz-InN (Ref. 2) and consistent with previous theoretical predictions,[4] providing some justification of the theoretical calculations. Detailed experimental studies of the electronic structure are still, however, somewhat lacking.

X-ray photoemission spectroscopy (XPS) has been shown to yield valence band spectra that closely resemble the total valence band density of states (VB-DOS) for many III-V and II-VI compounds,[13,14] including wz-InN(0001),[15] due to the high energy of the incident photons utilized in the measurements. This results in an approximately flat final density of states for excitation of photoelectrons, allowing the *k*-selection rule to be fulfilled without the introduction of additional structure due to final state modulations.

Here, this technique is applied to determine the VB-DOS of zb-InN, and this is compared with theoretical calculations employing quasiparticle corrected density functional theory (QPC-DFT) and with the VB-DOS of wz-InN.

II. EXPERIMENTAL AND THEORETICAL DETAILS

The zb-InN(001) was grown by plasma assisted molecular beam epitaxy (PAMBE) at a growth temperature of ~420 °C on a 3*C*-SiC(001) substrate incorporating a zb-GaN buffer layer. The InN layer thickness is ~80 nm, and is estimated to be 95% cubic phase. Details of the growth are reported elsewhere.[7] The wz-InN($11\bar{2}0$) (*a*-plane) was grown by PAMBE at a growth temperature of ~470 °C on an *r*-plane ($1\bar{1}02$) sapphire substrate incorporating an AlN buffer layer. The InN layer thickness is ~2600 nm.

High-resolution XPS measurements were performed using a Scienta ESCA300 spectrometer at the National Centre for Electron Spectroscopy and Surface Analysis, Daresbury

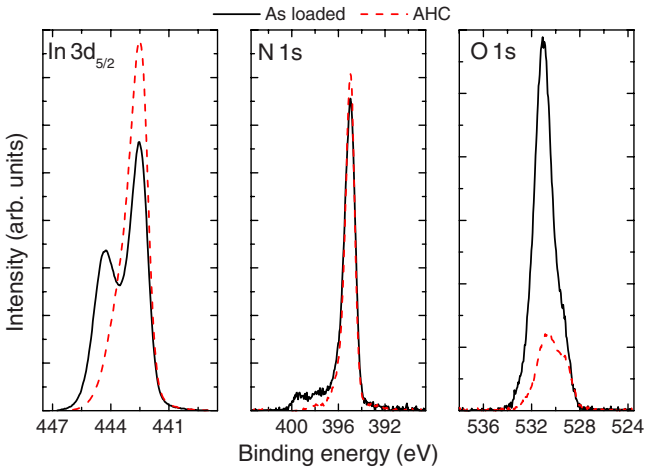

FIG. 1. (Color online) Shirley-background-subtracted In $3d_{5/2}$, N 1*s*, and O 1*s* zb-InN XPS core-level spectra, normalized to the In peak intensity, before (solid line) and after (dashed line) surface preparation by AHC as described in the text. The binding energy scale is given with respect to the VBM.

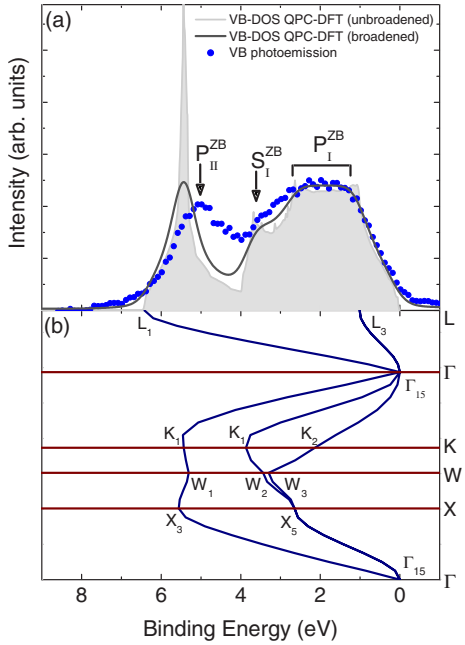

FIG. 2. (Color online) (a) Shirley-background-subtracted valence band photoemission spectrum and QPC-DFT VB-DOS shown without (shaded) and with lifetime and instrumental broadening for zb-InN. The main features in the VB-DOS are identified after Ley *et al.* (Ref. 14). The measured valence band photoemission is rigidly shifted to lower energies by 1.38 eV to align the VBM at 0 eV binding energy as for the calculations. The XPS and QPC-DFT spectra are normalized to the plateau P_I^{ZB} intensity. The corresponding QPC-DFT valence band structure for zb-InN is shown in (b), with high symmetry points denoted using double group symmetry notation.

Laboratory, UK. X-rays, of energy $h\nu = 1486.6$ eV, were produced using a monochromated rotating anode Al $K\alpha$ x-ray source. The ejected photoelectrons were analyzed by a 300 mm mean radius spherical-sector electron energy analyzer with 0.8 mm slits at a pass energy of 150 eV. The effective instrumental resolution is 0.45 eV, derived from the Gaussian convolution of the analyzer broadening and the natural linewidth of the x-ray source (0.27 eV). The binding energy scale is measured with respect to the Fermi level and was calibrated using the Fermi edge of an ion-bombarded silver reference sample that is regularly used to calibrate the spectrometer. A sample-dependent shift was subsequently applied to define the zero of the binding energy scale as the valence band maximum (VBM) in all cases.

The DFT calculations were performed using the hybrid functional HSE03 for exchange and correlation.[16] The electron-ion interaction was treated in the framework of the projector-augmented wave method, taking into account the In 4*d* electrons as valence states. Quasiparticle effects were included in the calculation of the DOS by a G_0W_0 correction of the generalized Kohn-Sham eigenvalues. Details of the calculations are reported elsewhere.[17] For comparison with the experimental results, the QPC-DFT DOS is broadened by a 0.2 eV full width at half maximum (FWHM) Lorentzian and a 0.45 eV FWHM Gaussian to account for lifetime and instrumental broadening, respectively.

InN surface preparation was performed under ultrahigh vacuum, in a preparation chamber connected to the XPS analysis chamber, using atomic hydrogen cleaning (AHC) which has previously been shown to clean InN surfaces without introducing electronic damage.[18] The sample was annealed at 200 °C under exposure to a 10 kL (1 L $= 10^{-6}$ Torr s) dose of molecular hydrogen passed through a thermal gas cracker with a cracking efficiency of approximately 50%, followed by a 1 h anneal at 275 °C. Core-level XPS measurements were taken before and after the AHC procedure, and are shown for the zb-InN in Fig. 1. Before treatment, a large O signal is observed, with a corresponding significant oxide component in the In and N core-level peaks chemically shifted to higher binding energies. The surface oxide is seen to be substantially reduced with AHC treatment. Similar results were obtained for the wz-InN sample.

III. RESULTS

Valence band photoemission from zb-InN(001) is shown in Fig. 2(a) after a Shirley background has been subtracted. Also shown are QPC-DFT VB-DOS calculations with and without lifetime and instrumental broadening. The surface Fermi level (zero of the binding energy scale in the measured XPS spectra) has been observed to be pinned 1.38 ± 0.10 eV above the VBM.[19] In contrast, the zero of energy is defined as the VBM in the QPC-DFT calculations. To allow accurate comparison between the experimental and theoretical results, the valence band photoemission spectrum has been shifted to lower energies by 1.38 eV to define the zero of the binding energy scale as the VBM for both the experimental and theoretical spectra.

The VB-DOS can be characterized by three main features: a plateau, a peak at slightly higher binding energies than the plateau, and a separate peak at higher binding energies still (marked P_I^{ZB}, S_I^{ZB}, and P_{II}^{ZB} in Fig. 2, respectively). The un-

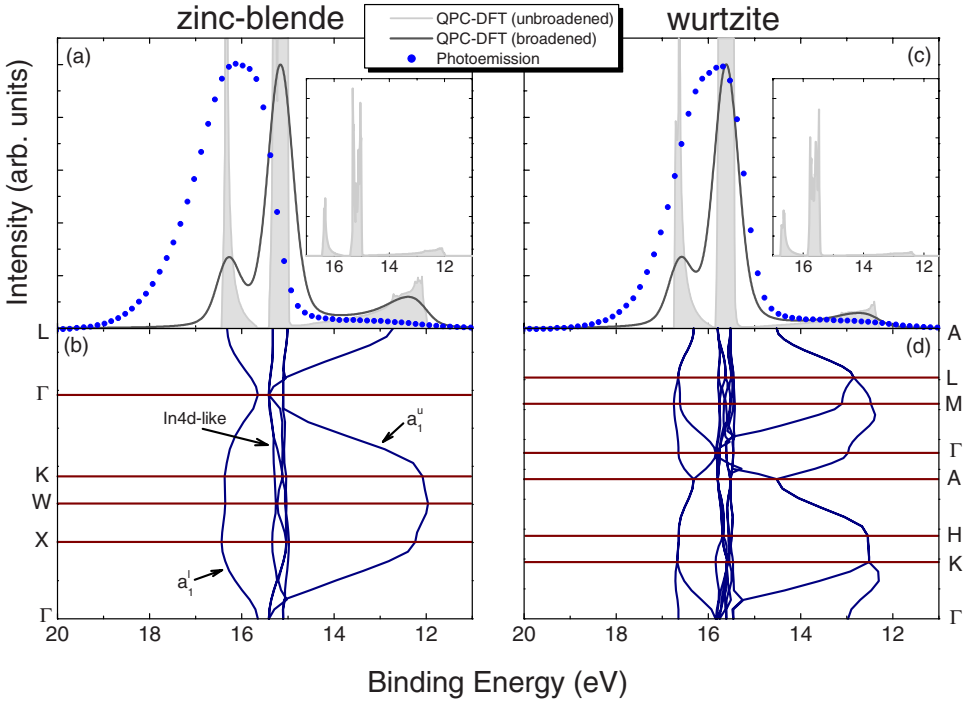

FIG. 3. (Color online) Shirley-background-subtracted photoemission spectrum around the In 4*d* XPS peak and QPC-DFT DOS calculations shown without (shaded) and with lifetime and instrumental broadening for (a) zb- and (c) wz-InN, and the corresponding QPC-DFT band structure calculations [(b) and (d)]. The measured XPS spectra are rigidly shifted to lower energies by 1.38 and 1.53 eV for the zb- and wz-InN, respectively, to align the VBM at 0 eV binding energy as for the calculations, and the XPS and QPC-DFT spectra are normalized to the In 4*d*-like peak intensity. The unbroadened DOS is shown in the inset over an extended intensity range.

derlying mechanisms giving rise to these features will be discussed in Sec. IV. When lifetime and instrumental broadening are included, the peak S_I^{ZB} becomes a shoulder on the plateau region. The experimental and theoretical VB-DOS show good agreement. In particular, the plateau P_I^{ZB} and the shoulder S_I^{ZB} occur at the same energies and very similar relative intensities in the XPS and QPC-DFT spectra. The peak P_{II}^{ZB} occurs at slightly lower binding energies in the XPS than in the QPC-DFT spectra, and also at a slightly lower intensity but larger width.

The presence of these three main regions in the VB-DOS is consistent with the observations of valence band features in many III-V semiconductors by Ley *et al.*[14] They also observed a peak at higher binding energies, P_{III}; however, in the present case, this is complicated by the relative location of the In 4*d* and N 2*s* levels. This region is shown in Fig. 3(a). The agreement between the QPC-DFT DOS calculations and the XPS spectrum is less good in this region, both in terms of the energy position of the main peak and the width of the features (the experimental spectrum occurs at higher binding energies and with much larger width than the QPC-DFT calculations). However, this feature contains both VB-DOS characteristics and also shallow core-level characteristics, and this will be discussed in further detail in Sec. IV.

For comparison, valence band photoemission from wz-InN($11\bar{2}0$) is shown in Fig. 4(a), again after a Shirley background has been subtracted. The surface Fermi level has been seen to be pinned 1.53 ± 0.10 eV above the VBM for wz-InN[19]; this shift has, therefore, been applied to the measured valence photoemission to align the XPS and QPC-DFT spectra as for the zb-InN.

Again, three main features are observed in the VB-DOS: two peaks (P_I^{WZ} and P_{II}^{WZ} in Fig. 4) and a shoulder (S_I^{WZ} in Fig. 4) on peak P_I^{WZ}, similar to the zb-InN and, more generally, to many other III-V semiconductors.[14] Comparison between the XPS and QPC-DFT spectra again reveals good general agreement, although peak P_{II}^{WZ} and the shoulder S_I^{WZ} occur at slightly lower binding energies in the XPS than in the QPC-DFT spectra. The intensity ratio of the two peaks (P_I^{WZ} and P_{II}^{WZ}) is similar between the XPS and QPC-DFT. This intensity ratio is known to vary between XPS measurements performed on different surface orientations of wz-InN.[20,21] The agreement here suggests that the nonpolar *a*-plane InN sample considered here most accurately represents the bulk VB-DOS.

The P_{III}^{WZ} region in the DOS is shown for wz-InN in Fig. 3(c). Again, the agreement between the QPC-DFT DOS calculations and the XPS spectrum is less good than at lower binding energies, with the experimental spectrum occurring at slightly higher binding energies and with much larger width than the QPC-DFT calculations, although the agreement is better than for zb-InN.

IV. DISCUSSION

The features of the zb-InN VB-DOS [Fig. 2(a)] can be understood from the calculated valence band structure [Fig. 2(b)]. In the zinc-blende structure, the atoms are tetrahedrally bonded with eight valence electrons per unit cell. In a simple tight-binding picture, these form four doubly spin-degenerate bands of *p*-orbital character (the three highest bands) and of *s*-orbital character. The Γ_{15} point marks the VBM where the three *p* bands are degenerate, neglecting spin-orbit splitting. Including the spin-orbit interaction splits the bands into a fourfold (including spin) degenerate band and a twofold degenerate band with Γ_8 and Γ_7 symmetry, respectively. However, the spin-orbit splitting is very small in InN,[22] and so will not be considered here. Γ_{15} therefore corresponds to the onset of the VB-DOS intensity, at 0 eV in the QPC-DFT calculations.

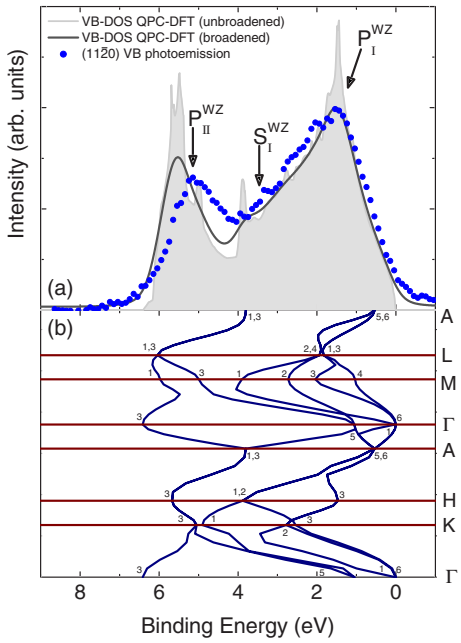

FIG. 4. (Color online) (a) Shirley-background-subtracted valence band photoemission spectrum and QPC-DFT VB-DOS shown without (shaded) and with lifetime and instrumental broadening for wz-InN. The main features in the VB-DOS are identified after Ley *et al.* (Ref. 14). The measured valence band photoemission is rigidly shifted to lower energies by 1.53 eV to align the VBM at 0 eV binding energy as for the calculations. The XPS and QPC-DFT spectra are normalized to the peak P_I^{WZ} intensity. The corresponding QPC-DFT valence band structure for wz-InN is shown in (b). High symmetry points are denoted using double group symmetry notation, although the symmetry point label has been dropped for clarity of presentation. Therefore, for example, at the valence band maximum, the label 6 denotes Γ_6 symmetry.

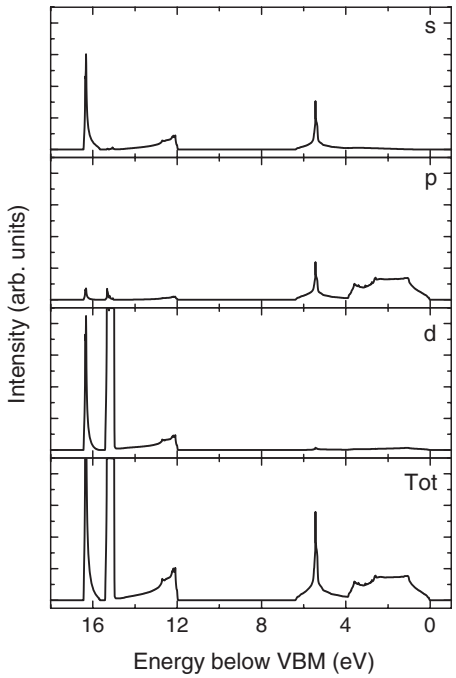

FIG. 5. *s*, *p*, and *d* resolved and total VB-DOS from QPC-DFT calculations for zb-InN.

The DOS is defined[23] as

$$g_n(E) = \int_{S_n(E)} \frac{dS}{4\pi^3} \frac{1}{|\nabla E_n(\mathbf{k})|}, \tag{1}$$

where E_n is the energy of band n, and S denotes a constant energy contour. Regions where the bands become flat in $\mathbf{k}$ space, therefore, lead to a large density of states, and in particular, critical points in the band structure such that $|\nabla E|=0$ cause van Hove singularities in the DOS.

Due to the relatively flat nature of the bands around Γ_{15}, the DOS rises rapidly below the VBM, peaking around the critical point L_3. However, between this point and X_5, the bands are approximately linear in $\mathbf{k}$, leading to a rather constant DOS and the plateau observed (P_I^{ZB}). A peak associated with X_5 is often observed in the DOS,[14] and indeed can be seen here in the unbroadened QPC-DFT calculations. However, this is not resolvable after broadening has been applied to the QPC-DFT or, consequently, in the photoemission spectra where the broadening is inherent. The peak S_I^{ZB} arises from the turning points in the band structure around K_1, and is broadened into a shoulder on the peak P_I^{ZB}. The good agreement between the features P_I^{ZB} and S_I^{ZB} in the broadened QPC-DFT and photoemission DOS results indicates the accuracy of the valence band calculations within ~4 eV of the VBM. The QPC-DFT VB-DOS calculations can be resolved into *s*-, *p*-, and *d*-orbital components, and these are shown in Fig. 5. Clearly, the DOS in this $\lesssim$4 eV region is almost entirely *p*-orbital-like, as expected from simple tight-binding arguments.

The points X_3, W_1, and K_1 are almost degenerate in the band structure. An intense but narrow peak, therefore, results in the DOS (P_{II}^{ZB}). This is considerably reduced in intensity and increased in width by lifetime and instrumental broadening. The experimental peak occurs at slightly lower binding energies than in the QPC-DFT DOS, suggesting that X_3, W_1, and K_1 occur at slightly too high binding energies in the calculations. It should be noted that in the XPS measurements discussed so far, final state relaxations have been ignored. Such effects can cause features to shift toward the VBM.[14] However, it is unlikely to be a large effect for these binding energies, as the bands here do not have significant core-like character. The peak P_{II}^{ZB} is also broader in the experimental spectrum than in the (broadened) theoretical calculations. Lifetime broadening is known to increase with increasing binding energy.[14] This has not been included in the broadening applied to the QPC-DFT calculations, and so may explain the extra broadening observed in peak P_{II}^{ZB}. The bottom of peak P_{II}^{ZB} is determined in this case by the point L_1, which is the lowest point of the third valence band. An extrapolation of the trailing edge of the experimental P_{II}^{ZB} peak to the baseline to take account of instrumental and lifetime broadening effects indicates good agreement with the edge of peak P_{II}^{ZB} in the experimental VB-DOS spectrum with L_1.

From tight-binding arguments, the fourth valence band is expected to be of largely anion (N) *s*-orbital character, and is separated from the other three valence bands by an energy

gap dependent on the ionicity of the semiconductor, the so-called ionicity gap.[13,14] Due to the large electronegativity difference of In and N, InN has a large ionicity gap; indeed, the N 2*s* orbital is located close in energy to the In 4*d* orbital.[24] At **k** points away from Γ, the In 4*d* orbital and N 2*s* orbital symmetries both support the irreducible representation a_1, creating an a_1-a_1 (*s*-*d*) repulsion.[10] Due to the proximity of the N 2*s* and In 4*d* orbital energies, the *s*-*d* coupling is strong, and the *s*-orbital valence band splits into an upper (a_1^u) and a lower (a_1^l) band, with the In 4*d* band between.[10] This is evident in the QPC-DFT band structure in Fig. 3(b).

The In 4*d* orbitals are somewhat core-like, and so quite localized in real space. The corresponding bands are, therefore, narrow in energy, leading to a narrow and very intense peak in the DOS (significantly more intense than any of the valence band features) although it is reduced in intensity by broadening effects. In the lower split-off band a_1^l, the *X*, *K*, *L*, and *W* points are almost degenerate in energy, leading to another sharp and fairly intense peak in the DOS, whereas the upper band a_1^u is more extended. The top of this band occurs at *W*, where the *s*-*d* repulsion is large, leading to the onset of intensity in the DOS seen in Fig. 3(a). The *s*-*d* hybridization is, however, symmetry forbidden at Γ (Ref. 10) and so the splitting of the a_1^u and a_1^l bands tends to zero here. This leads to the rather extended a_1^u band, and hence a broad peak in the DOS corresponding to this. From the *s*, *p*, and *d* resolved DOS (Fig. 5), the peak attributed to the In 4*d* bands clearly has almost entirely *d*-like character, consistent with this explanation. The two peaks in the DOS due to the a_1^u and a_1^l bands have both *s*- and *d*-orbital (and a small amount of *p*-orbital) character due to their coupled nature.

Comparison of the experimental photoemission spectrum with the QPC-DFT DOS calculations in this region is complicated by a number of factors. First, as discussed previously, lifetime broadening increases with increasing binding energy, which is not accounted for in the broadening of the QPC-DFT DOS; considerable lifetime broadening has previously been observed in the anion 2*s* peak in the DOS of ionic compounds.[14] This likely accounts for some of the extra broadening observed here in the photoemission compared to the calculations. Second, the cross section for photoemission varies with energy, atomic species of the host, and orbital type, and so this causes variation in the intensity of the features from that expected from the QPC-DFT calculations alone. The cross section for N 2*s* electrons is significantly lower than for In 4*d* electrons, and so the intensity ratio of the In 4*d* peak to the a_1^l or a_1^u peaks would be expected to be greater in the photoemission than in the QPC-DFT DOS. This is clearly observable for the a_1^u peak, which occurs at much lower intensities in the XPS spectrum than in the QPC-DFT DOS. Third, core-level peaks in XPS spectra of InN are known to exhibit an asymmetric high-binding-energy tail due to inelastic losses to conduction band plasmons.[25] This further broadens the high-binding-energy side of the In 4*d* peak.

QPC-DFT calculations utilizing the HSE03 hybrid functional are known[17] to underestimate the *d*-band binding energies in zb-InN; this is evident when comparing the XPS with the QPC-DFT spectra in this region. This will also lead (due to the *s*-*d* coupling) to small errors in the binding energies of the DOS features due to the a_1^u and a_1^l bands. There is an (weak) onset in photoemission intensity at binding energies below the main In 4*d* peak. This is attributed to the a_1^u band. The main peak also has a marked asymmetry with a high-binding-energy tail. This is attributed to the combined effects of inelastic losses to conduction band plasmons[25] and to emission from the a_1^l band, suggesting the presence of *s*-*d* hybridized bands. The large width and limited resolution, however, limit the information attainable about this hybridization.

The wurtzite and zinc-blende structures are both tetrahedrally bonded configurations, differing only to third nearest neighbor. As the environment immediately surrounding each atom is so similar for the two structures, the VB-DOS for zb- and wz-InN would be expected to be similar. This is indeed the case, with the VB-DOS described by peaks P_I and P_{II} with a shoulder S_I on peak P_I in both cases. The valence band structure [Fig. 4(b)] is, however, significantly more complex for the wz than the zb polymorph due to the anisotropic nature of the wurtzite structure, which leads to a nonzero crystal field splitting, and the differing shapes of the Brillouin zones for the two structures. The threefold degeneracy (neglecting spin) of the valence bands at Γ is lifted by the presence of this crystal field, and these split into two degenerate bands with Γ_6 symmetry which define the VBM, located above a third band (with Γ_1 symmetry) by an energy equal to the crystal field splitting. Each of these three bands is also doubly degenerate due to spin, and including the spin-orbit interaction lifts the degeneracy of the top two valence bands. However, as for zb-InN, the small spin-orbit splitting will not be considered further.

The onset of the VB-DOS, therefore, corresponds to Γ_6. Instead of rising to a plateau (as for zb-InN), the DOS continues to rise rapidly due to a number of turning points in the band structure (such as Γ_5, $A_{5,6}$, and M_4). The peak P_I^{WZ} occurs at the coincidence of the critical points at H_3 and in the *L*-*M* direction between $L_{1,3}$ and M_3. After falling off, the DOS peaks again (S_I^{WZ}) due to the near degeneracy of $H_{1,2}$ and $A_{1,3}$, although when lifetime and instrumental broadening are applied, this is broadened into a shoulder on P_I^{WZ}. A number of turning points in the band structure ~2–3 eV below the VBM lead to several small peaks in the unbroadened QPC-DFT calculations between P_I^{WZ} and S_I^{WZ}, although these features are very poorly resolved when broadening has been applied. Some additional intensity is observable in the XPS spectrum at these binding energies, and this may be due to these small peaks in the DOS, implying a slight underestimation of their intensity in the calculations; however, this is difficult to confirm.

The second predominant peak, P_{II}^{WZ}, occurs largely due to the critical points at H_3 and in the Σ (Γ-*M*) direction between Γ_3 and M_1. Both the shoulder S_I^{WZ} and peak P_{II}^{WZ} occur at slightly lower binding energies in the experimental compared to the theoretical spectra, indicating a slight overestimation of the binding energies of the specified critical points in the QPC-DFT calculations. The peak P_{II}^{WZ} is also broader in the experimental than in the theoretical spectra, as for zb-InN, again indicating the influence of increasing lifetime broadening with increasing binding energy that has not been included in broadening the QPC-DFT calculations. From Fig. 6, it is again clear that the VB-DOS at low binding

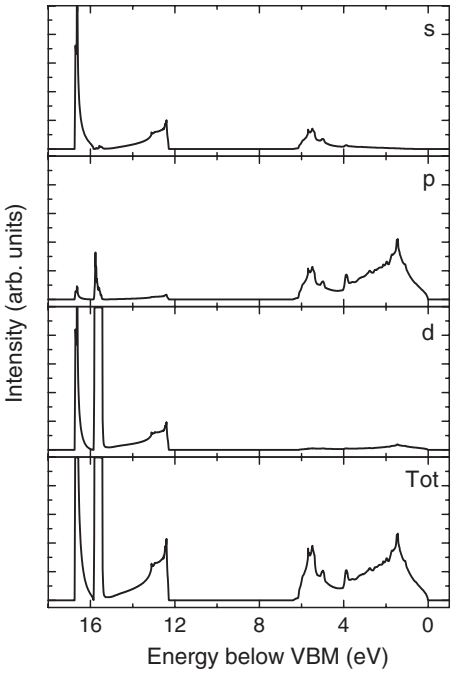

FIG. 6. *s*, *p*, and *d* resolved and total VB-DOS from QPC-DFT calculations for wz-InN.

energies is almost entirely *p* like, although with a small admixture of *s*-like states around P_{II}^{WZ}, as for the zb-InN VB-DOS. The edge of peak P_{II}^{WZ} is defined by Γ_3. Extrapolating the trailing edge of the XPS spectrum of peak P_{II}^{WZ} to the baseline gives an energy in agreement with the position of Γ_3, marking the high-binding-energy onset of peak P_{II}^{WZ}.

It should be noted that some intensity is present in the experimental spectrum at binding energies below Γ_6 (below the onset of the bulk DOS), which extends all the way to the Fermi level. This can be identified as due to photoemission from surface In adlayers, which have been theoretically predicted[26] and experimentally observed[20,21] to occur as the energetically favorable surface reconstruction for wz-InN surfaces under In-rich conditions. These In adlayers give rise to a surface DOS markedly different from that of the bulk,[27] which has been attributed[27,28] as the microscopic origin of the electron accumulation present at InN surfaces. Due to the high energy of the incident x-rays in XPS and the corresponding high kinetic energy of ejected photoelectrons, the photoelectron escape depth is significantly larger than the surface adlayer region, allowing the features of the bulk DOS to be clearly identified. These are, however, slightly modified by the contribution of the surface DOS, as seen by the photoemission below the onset of the bulk DOS and the polarity dependence of the valence photoemission observed previously.[19,20]

The higher binding energy region of the DOS around the In 4*d* levels [Fig. 3(c)] is again similar to that of zb-InN. The narrow In 4*d* bands give rise to a narrow intense peak in the DOS, and the *s*-*d* hybridization again splits the N 2*s*-like level into upper and lower bands, giving peaks in the DOS above and below the In 4*d* peaks. The In 4*d*-like nature of the central peak and coupled *s*-*d* nature of the surrounding peaks are confirmed by the *s*, *p*, and *d* resolved DOS (Fig. 6), similar to that of zb-InN, although there is a slightly higher admixture of *p*-like contributions for wz-InN. The energy alignment of the QPC-DFT and XPS spectra is better in this case than for the zb-InN, although the *d*-band binding energies are still slightly underestimated in the QPC-DFT calculations. The onset of photoemission at binding energies below the main peak and the extent of the high-binding-energy tail to the main peak give evidence for an *s*-*d* hybridization in wz-InN also. The experimental peaks are also significantly broader than the calculated DOS, again suggesting the influence of the increase in lifetime broadening with increasing binding energy.

V. CONCLUSIONS

The valence band density of states of zinc-blende InN(001) has been measured by x-ray photoemission spectroscopy. The VB-DOS was characterized by three main regions: a plateau region after the initial rise in the DOS, followed by a shoulder on this region and a second narrow but intense peak. This is consistent with previous investigations of the VB-DOS of III-V and II-VI semiconductor compounds. The measured VB-DOS was compared to theoretical calculations performed using density functional theory employing the hybrid functional HSE03 for exchange and correlation, and including quasiparticle effects by a G_0W_0 correction of the generalized Kohn-Sham eigenvalues. Agreement was observed between the XPS and QPC-DFT VB-DOS, and the features in the DOS were related to distinct features in the calculated band structure.

At higher binding energies, an *s*-*d* coupling is expected from the QPC-DFT calculations between the In 4*d* and the N 2*s* orbitals, leading to a splitting of the *s* band (from a simple tight-binding picture) into upper and lower *s*-*d* hybridized bands located around the In 4*d* bands. The experimental measurements support this conclusion, although significant broadening (attributed to an increase in lifetime broadening with increasing energy), variation in cross section for photoemission, and the presence of inelastic loss features make detailed comparison of the XPS with the QPC-DFT DOS difficult in this region.

XPS measurements of the wurtzite InN($11\bar{2}0$) VB-DOS and corresponding QPC-DFT calculations were also presented. The VB-DOS was seen to be similar to that of zb-InN, consisting of two peaks with a shoulder on the lower binding energy peak, due to the similarities of the wurtzite and zinc-blende crystal structures. Spectral intensity above the valence band maximum was observed, attributed to photoemission from surface metal-adlayer reconstructions. Evidence of *s*-*d* splitting was again observed at higher binding energies.

ACKNOWLEDGMENTS

We are grateful to D. Law and G. Beamson of NCESS for their assistance with XPS measurements, and H. Nagasawa and M. Abe from SiC Development Center, HOYA Corporation, Japan for supplying the 3C-SiC substrates. Also, we

acknowledge the Engineering and Physical Sciences Research Council, UK, for financial support under Grant No. EP/C535553/1 and access to the NCESS facility under Grant No. EP/E025722/1, and the Deutsche Forschungsgemeinschaft for financial support under Project No. Be1346/18-2.

*c.f.mcconville@warwick.ac.uk

†Present address: Department of Physics, Nanjing University, Nanjing 210093, China.

[1] V. Yu. Davydov, A. A. Klochikhin, R. P. Seisyan, V. V. Emtsev, S. V. Ivanov, F. Bechstedt, J. Furthmuller, H. Harima, V. Mudryi, J. Aderhold, O. Semchinova, and J. Graul, Phys. Status Solidi B **229**, R1 (2002).

[2] J. Wu, W. Walukiewicz, W. Shan, K. M. Yu, J. W. Ager III, S. X. Li, E. E. Haller, H. Lu, and W. J. Schaff, J. Appl. Phys. **94**, 4457 (2003).

[3] V. M. Polyakov and F. Schwierz, Appl. Phys. Lett. **88**, 032101 (2006).

[4] J. Furthmüller, P. H. Hahn, F. Fuchs, and F. Bechstedt, Phys. Rev. B **72**, 205106 (2005).

[5] A. Tabata, A. P. Lima, L. K. Teles, L. M. R. Scolfaro, J. R. Leite, V. Lemos, B. Schöttker, T. Frey, D. Schikora, and K. Lischka, Appl. Phys. Lett. **74**, 362 (1999).

[6] P. A. Anderson, C. E. Kendrick, R. J. Kinsey, A. Asadov, W. Gao, R. J. Reeves, and S. M. Durbin, Phys. Status Solidi C **2**, 2320 (2005).

[7] J. Schörmann, D. J. As, K. Lischka, P. Schley, R. Goldhahn, S. F. Li, W. Löffler, M. Hetterich, and H. Kalt, Appl. Phys. Lett. **89**, 261903 (2006).

[8] J. G. Lozano, F. M. Morales, R. Garcia, D. Gonzalez, V. Lebedev, Ch. Y. Wang, V. Cimalla, and O. Ambacher, Appl. Phys. Lett. **90**, 091901 (2007).

[9] F. Bechstedt and J. Furthmüller, J. Cryst. Growth **246**, 315 (2002).

[10] C. Persson and A. Zunger, Phys. Rev. B **68**, 073205 (2003).

[11] D. Fritsch, H. Schmidt, and M. Grundmann, Phys. Rev. B **69**, 165204 (2004).

[12] P. Rinke, M. Scheffler, A. Qteish, M. Winkelnkemper, D. Bimberg, and J. Neugebauer, Appl. Phys. Lett. **89**, 161919 (2006).

[13] R. A. Pollak, L. Ley, S. Kowalczyk, D. A. Shirley, J. D. Joannopoulos, D. J. Chadi, and M. L. Cohen, Phys. Rev. Lett. **29**, 1103 (1972).

[14] L. Ley, R. A. Pollak, F. R. McFeely, S. Kowalczyk, and D. A. Shirley, Phys. Rev. B **9**, 600 (1974).

[15] L. F. J. Piper, T. D. Veal, P. H. Jefferson, C. F. McConville, F. Fuchs, J. Furthmüller, F. Bechstedt, H. Lu, and W. J. Schaff, Phys. Rev. B **72**, 245319 (2005).

[16] J. Heyd, G. E. Scuseria, and M. Ernzerhof, J. Chem. Phys. **118**, 8207 (2003).

[17] F. Fuchs, J. Furthmüller, F. Bechstedt, M. Shishkin, and G. Kresse, Phys. Rev. B **76**, 115109 (2007).

[18] L. F. J. Piper, T. D. Veal, M. Walker, I. Mahboob, C. F. McConville, H. Lu, and W. J. Schaff, J. Vac. Sci. Technol. A **23**, 617 (2005).

[19] P. D. C. King, T. D. Veal, C. F. McConville, F. Fuchs, J. Furthmüller, F. Bechstedt, P. Schley, R. Goldhahn, J. Schörmann, D. J. As, K. Lischka, D. Muto, H. Naoi, Y. Nanishi, Hai Lu, and W. J. Schaff, Appl. Phys. Lett. **91**, 092101 (2007).

[20] T. D. Veal, P. D. C. King, P. H. Jefferson, L. F. J. Piper, C. F. McConville, H. Lu, W. J. Schaff, P. A. Anderson, S. M. Durbin, D. Muto, H. Naoi, and Y. Nanishi, Phys. Rev. B **76**, 075313 (2007).

[21] T. D. Veal, P. D. C. King, M. Walker, C. F. McConville, H. Lu, and W. J. Schaff, Physica B **401-402**, 351 (2007).

[22] I. Vurgaftman and J. R. Meyer, J. Appl. Phys. **94**, 3675 (2003).

[23] N. W. Ashcroft and N. D. Mermin, *Solid State Physics* (Saunders College, Philadelphia, 1976).

[24] P. D. C. King, T. D. Veal, P. H. Jefferson, S. A. Hatfield, L. F. J. Piper, C. F. McConville, F. Fuchs, J. Furthmüller, F. Bechstedt, H. Lu, and W. J. Schaff, Phys. Rev. B **77**, 045316 (2008).

[25] P. D. C. King, T. D. Veal, H. Lu, S. A. Hatfield, W. J. Schaff, and C. F. McConville, Surf. Sci. **602**, 871 (2008).

[26] D. Segev and C. G. Van de Walle, Surf. Sci. **601**, L15 (2007).

[27] D. Segev and C. G. Van de Walle, Europhys. Lett. **76**, 305 (2006).

[28] C. G. Van de Walle and D. Segev, J. Appl. Phys. **101**, 081704 (2007).